N77-27076

A THREE-DIMENSIONAL VISCOUS/POTENTIAL FLOW INTERACTION ANALYSIS METHOD FOR MULTI-ELEMENT WINGS

NATIONAL AERONAUTICS AND SPACE ADMINISTRATION
WASHINGTON, DC

AUG 77

A THREE-DIMENSIONAL VISCOUS/POTENTIAL FLOW
INTERACTION ANALYSIS METHOD FOR MULTI-ELEMENT WINGS

F.A. Dvorak
F.A. Woodward
B. Maskew

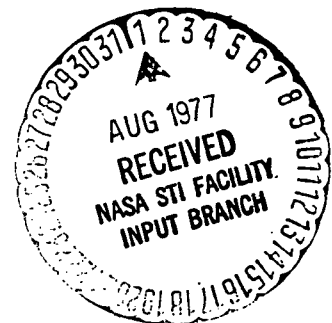JULY 1977

SUBMITTED TO:

NASA AMES RESEARCH CENTER
MOFFETT FIELD, CALIFORNIA 94035

CONTRACT NAS2-8788

ANALYTICAL METHODS, INC.
100 - 116TH AVENUE S.E.
BELLEVUE, WASHINGTON 98004
(206) 454-6119

ANALYTICAL METHODS REPORT No. 7603

TABLE OF CONTENTS

LIST OF FIGURES

A THREE-DIMENSIONAL VISCOUS/POTENTIAL FLOW
INTERACTION ANALYSIS METHOD FOR MULTI-ELEMENT WINGS

By

F.A. Dvorak, F.A. Woodward and B. Maskew
Analytical Methods, Inc.

SUMMARY

An analysis method and computer program have been developed
for the calculation of the viscosity-dependent aerodynamic charac-
teristics of multi-element, <u>finite</u> wings in incompressible flow.
This work is an extension to three dimensions of the method deve-
loped previously under Contract NAS2-7048, Reference 1. The
methods differ in that a fully three-dimensional potential flow
program is now used to determine the inviscid pressure distribu-
tion about the configuration. The potential flow program uses
surface source and vortex singularities to represent the inviscid
flow. The method is capable of analysing configurations having at
most one slat, a main element, and two slotted flaps. Currently,
the configurations are limited to full span slats or flaps. The
configuration wake is allowed to relax as a force-free wake, al-
though roll-up is not allowed at this time.

Once the inviscid pressure distribution is calculated, a
series of boundary layer computations are made along streamwise
strips. Each strip is treated as if it were a separate infinite
yawed wing; consequently, the boundary layer methods developed
in Reference 1 are used directly in the new program. Source dis-
tributions are determined along the streamwise strips from the
boundary layer and potential flow calculations. They are used to
modify the boundary conditions in the second and subsequent cal-
culations of the potential flow. These sources represent the

effect of the boundary layer in the modification of the potential flow. The sequence of potential flow and boundary layer calculations continue until convergence of the lift coefficient (usually 2 to 4 iterations). Lift, drag and pitching moment coefficients are then determined. The method is currently the only one of its kind capable of analyzing finite wings.

The computer program is written in Fortran IV for the CDC 6600 and 7600 family of computers. The program operates in the overlay mode, and requires an amount of storage dependent on the number of panels used to describe the configuration. Typically 300 panels will require about 170,000 (Octal) words of storage.

INTRODUCTION

Background

An analysis method has recently been developed which is capable of predicting the aerodynamic characteristics of infinite yawed multi-element wings (Ref. 1). The effect of viscosity is included in the calculation through the use of distributed sources determined from the boundary layer analysis. These sources are included in the subsequent potential flow calculation giving a viscosity dependent flow field. Convergence of the method as measured by lift coefficient is generally very rapid.

Application of the method for comparison with experiment has demonstrated its validity for a wide range of problems. One such case is the optimization of flap-gap and overlap for a multi-element configuration resulting in maximum lift for a given angle-of-attack. An extended version of the method (Ref. 2) has been coupled with an optimization program for use in determining the optimum slat locations for maximum lift.

Because most aerodynamic flows of interest are three dimensional in nature, the ability to consider the effect of finite span on such parameters as flap-gap is very desirable. A fully three-dimensional method would have many applications important to the designer of modern high-lift systems. Its availability would greatly reduce the reliance on the experimental method. Development of such a method was consequently undertaken, and the resulting procedure is described in this report.

Problem Definition

The calculation of the potential flow field about a general three-dimensional multi-element wing (see Figure 1) represents the first task of any analysis method. Because of the complex

nature of the configurations likely to be analysed, a geometry
control program will be an essential feature of the overall method.
As in the case of Program VIP (Ref. 1), the potential flow method
must be capable of predicting the pressure distribution at selec-
ted off-body points above the flap elements. An additional requ-
irement in the three-dimensional case is a wake representation
capable of providing for wake roll-up and ultimately for tip-edge
vortex roll-up. In three dimensions these effects become impor-
tant at relatively low lift coefficients.

With the potential flow field specified, it is necessary to
predict the boundary layer development over the multi-element con-
figuration. Calculations must include stagnation line initial
conditions, laminar, transition and turbulent boundary layer deve-
lopments and laminar or turbulent separation predictions for each
element of the wing high-lift system. The calculations must in-
clude accurate predictions of boundary layer development in the
regions where wing or first flap upper surface and cove boundary
layers merge with the downstream flap upper surface boundary layer.
Both longitudinal curvature and normal pressure gradient terms
must be included in the governing boundary layer equations as each
effect has a significant influence on the boundary layer develop-
ment, and subsequently on the section drag coefficient. These
effects are particularly important in the wing trailing-edge/flap
leading-edge region. Once the boundary layer development is known,
its effect on the external flow must be determined.

A complete analysis program for the aerodynamic characteris-
tics of general three-dimensional multi-element wings is developed
by combining the separate goemetry, potential flow and boundary
layer calculation procedures. Iteration between the separate pro-
grams results in the prediction of viscosity-dependent aerodyna-
mic forces. The different calculation schemes that form the

4

elements of the integrated computer program are discussed in the following sections.

LIST OF SYMBOLS

a_{ij}	Aerodynamic influence coefficient
b_{ij}	Normal velocity due to external source
C^*	Reynolds number at stagnation line
C_D	Profile drag coefficient $= \dfrac{D}{\frac{1}{2}\rho U_\infty^2 c}$
C_L	Lift coefficient $= \dfrac{L}{\frac{1}{2}\rho U_\infty^2 c}$
C_M	Moment coefficient
c	Airfoil normal chord
c_f	Local skin friction coefficient
C_p	Pressure coefficient
D	Drag force/unit span
H	Shape factor, ratio of displacement to momentum thickness, (σ^*/θ)
K	Non-dimensional pressure gradient parameter
l, m, n	Direction cosines
L	Lift force/per unit span
M_L	Local Mach number
M_∞	Free stream Mach number
P	Static pressure, pounds per square inch absolute

5

q_i	Source strength
R_i	Total normal velocity
R_c	Chord Reynolds number $U_\infty c/\nu$
R_θ	Momentum thickness Reynolds number $U\theta/\nu$
$R_{\theta ins}$	Streamwise momentum thickness Reynolds number at instability point
$R_{\theta trans}$	Streamwise momentum thickness Reynolds number at transition
T_{ij}	Transformation matrix
U_S	Local streamwise velocity
U_∞	Free stream velocity
V	Tangential velocity at airfoil surface
u, v, w	Components of velocity in x, y and z directions
U_τ	Friction velocity $(\tau_w/\rho)^{\frac{1}{2}}$
x, y, z	Components of length in the chord, normal and span-wise directions
S	Distance along a streamline
ξ, η, ζ	Panel coordinate system
δ	Boundary layer thickness
ρ	Density of air
τ	Shear stress
τ_w	Local surface shear stress
γ_i	Vortex strength

α	Angle of attack
β	Angle of yaw
ν	Kinematic viscosity
ν_t	Eddy viscosity
$\gamma(y)$	Intermittency funciton
σ	Standard deviation of intermittency function

Subscripts

e	Value at edge of boundary layer
i	i^{th} value
in	Incompressible
ins	Instability
j	j^{th} value
L	Local value
l	lower
trans	Transition
s	Streamline component
t	Turbulent
u	Upper

POTENTIAL FLOW METHOD

Configuration Definition

A typical panel subdivision of a high-lift wing configuration is illustrated in Figure 1. A reference coordinate system is established with origin at or near the leading edge of the configuration, having an x axis lying in the plane of symmetry parallel to the streamwise axis, and a vertical z axis.

Each wing element may be specified in its own or in the reference coordinate system. Individual coordinate systems are related to the reference coordinate system by pivot points. The pivot points are prescribed in the reference coordinate system. In order to loft the configuration, element rotation angles must also be prescribed. Given the pivot points and rotation angles, any element may be translated and rotated to the desired location relative to the reference coordinate system.

Wing twist, taper and dihedral can be readily accommodated by the geometry control program.

If the wing configuration is made up of a main element and one or more slotted flaps, then additional analysis is required to determine flap upper surface longitudinal radius or curvature for later use in the finite difference boundary layer calculations. The spline technique as described in Reference 1 is used in the present method.

Each element of a multi-element wing configuration is represented by a series of streamwise airfoil sections given at selected intervals along the span. Planar surface panels are located between adjacent sections, with the corner points being defined by the section coordinates. The section coordinates may be given in percent chord or directly in terms of the reference coordinate

8

system. The panels in each wing section are generally numbered
sequentially from the trailing edge on the lower surface around
the leading edge to the trailing edge on the upper surface. The
same number of points at approximately the same percent chord
locations must be used to define the wing upper and lower surfaces.

Each chordwise strip of wing panels contains a constant vor-
tex distribution starting at the trailing edge of the lower sur-
face, around the leading-edge, and ending at the trailing edge of
the upper surface. These vortex strips are used to provide circu-
lation around lifting surfaces. One additional panel is defined
in the wake aft of each chordwise strip to provide control points
for satisfying the Kutta condition. The additional panel lies in
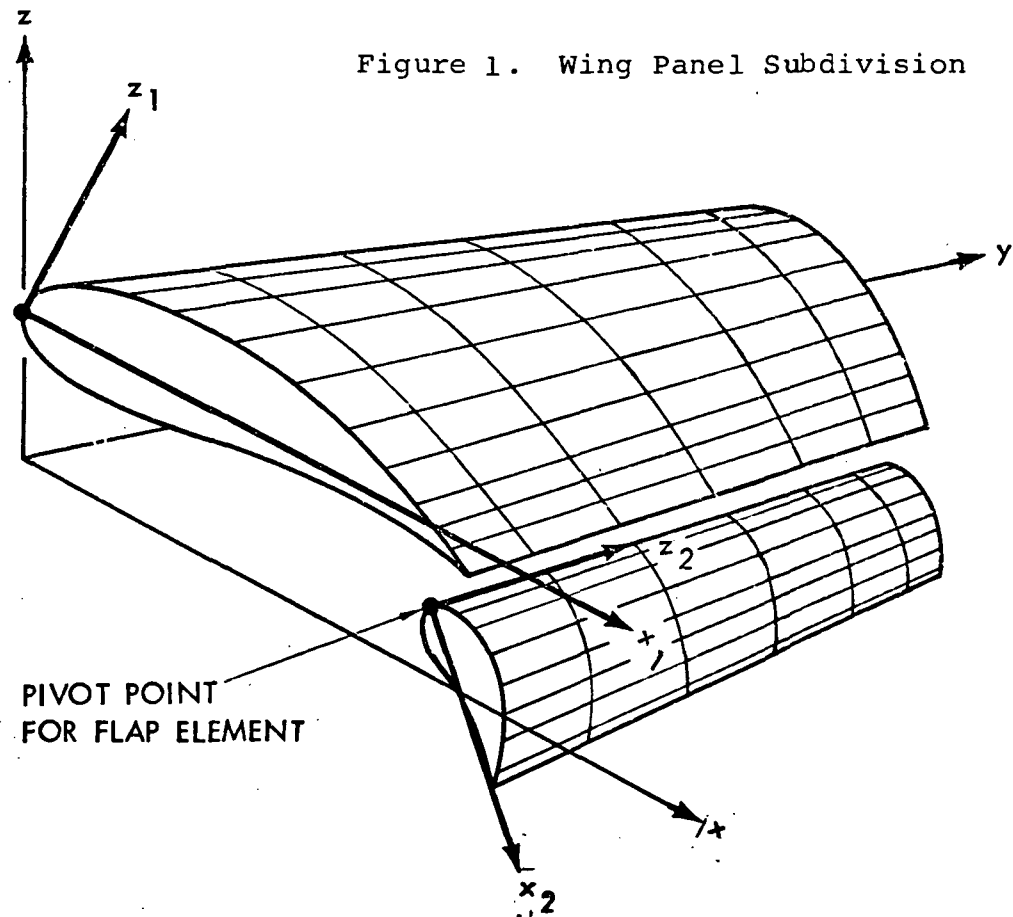the plane of the trailing edge bisector.

Figure 1. Wing Panel Subdivision

PIVOT POINT
FOR FLAP ELEMENT

Each panel is defined by four corner points. Since these four points may not lie in the same plane, an equivalent planar panel is generated using the method of Reference 3, the details of which are described in Appendix I. A panel coordinate system is defined which has its origin at the panel centroid. The ξ and η axes lie in the plane of the panel, while the ζ axis is perpendicular to that plane. The ξ axis is oriented such that the ξ, ζ plane is parallel to the reference x axis.
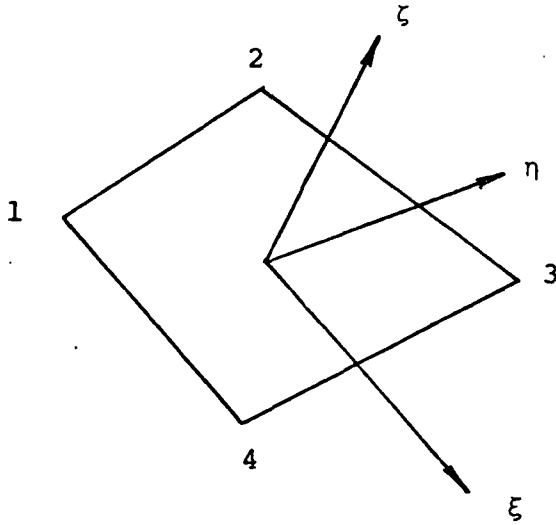
Figure 2. Panel Coordinate System

Since the velocity components induced by the source and vortex distributions are given in terms of the panel coordinate system, a nine-element transformation matrix, T_{ij}, is calculated for each panel to transform the coordinates of points and the components of vectors from the reference coordinate system to the panel

coordinate system. In addition, the panel area, the coordinates of the centroid, and the length of the principal diagonal are calculated.

Inviscid Flow Model

The surface of the configuration is subdivided into a large number of panels, each of which contains a constant source and constant vortex distribution. A concentrated vortex originates from the downstream corners of each vortex panel, and follows the wing contour along the inner and outer edges of each strip of panels until the trailing-edge is reached. Downstream of the trailing-edge, this system of vortices forms the trailing vortex wake.

Analytical expressions for the perturbation velocity field induced by a constant source distribution on an arbitrary quadrilateral panel are given by Hess and Smith (Ref. 3). Equivalent expressions for the perturbation velocities induced by a constant vortex distribution on the same arbitrary quadrilateral are given herein. The perturbation velocities are used to calculate the coefficients of a system of linear equations relating the magnitude of the normal velocities at the panel control points to the unknown source and vortex strengths. The source and vortex strengths which satisfy the boundary condition of tangential flow at the control points for a given Mach number and angle of attack are determined by solving this system of equations by an iterative procedure. Initially, the vortex wake is constrained to trail in the free stream direction during this solution procedure. However, an optional wake relaxation procedure is also available which allows the trailing vortices to move in a vertical direction and approximate the streamlines of the flow. Transverse movement of

the vortices is not permitted in order to avoid adverse interfe-
rence between the vortices and control points on downstream flap
elements. With this option, an additional iteration loop is super-
imposed on the basic solution procedure, in which the influence of
the wake on the wing is recalculated during each cycle. Complete
wake relaxation, including roll-up of the wing tip vortices, is
not permitted in order to minimize the number of iterations re-
quired for convergence.

The pressure coefficients at panel control points are calcu-
lated from the perturbation velocity components, and finally, the
forces and moments acting on the complete configuration are ob-
tained by numerical integration.

The Incompressible Velocity Components

The perturbation velocity components, u_x, v_x, and w_x, induced
by a constant source distribution on an arbitrary quadrilateral
panel are derived in Reference 3.

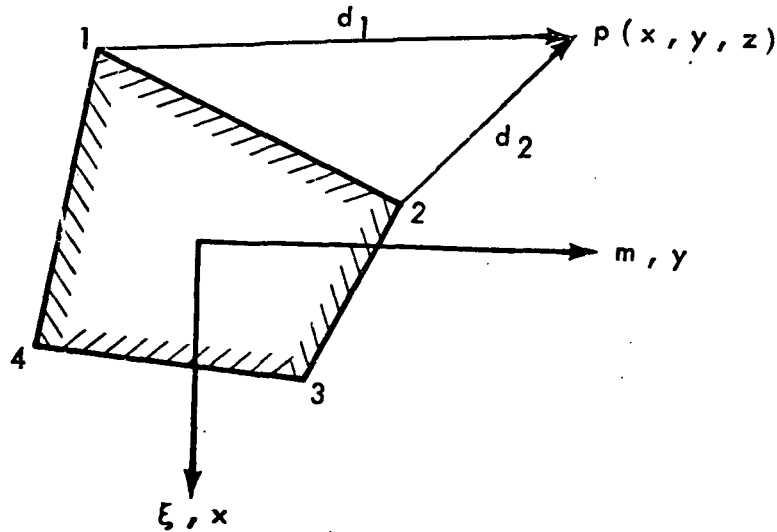The equations are given in terms of the panel coordinate
system.

Figure 3. Panel Geometry

The panel corner points are numbered in a clockwise direction. The perturbation velocities at an arbitrary point, $P(x,y,z)$, are given as the sum of the contributions of the four sides of the quadrilateral as follows.

$$u_s = -S_{12}G_{12} - S_{23}G_{23} - S_{34}G_{34} - S_{41}G_{41} \tag{1}$$

$$v_s = C_{12}G_{12} + C_{23}G_{23} + C_{34}G_{34} + C_{41}G_{41} \tag{2}$$

$$w_s = F_1 + F_2 + F_3 + F_4 \tag{3}$$

where

$$S_{12} = \frac{1}{\sqrt{1 + B_{12}^2}} \ , \ S_{23} = \frac{1}{\sqrt{1 + B_{23}^2}} \ , \ S_{34} = \frac{-1}{\sqrt{1 + B_{34}^2}} \ ,$$

$$S_{41} = \frac{-1}{\sqrt{1 + B_{41}^2}}$$

$$C_{12} = B_{12}S_{12} \ , \ C_{23} = B_{23}S_{23} \ , \ C_{34} = B_{34}S_{34} \ , \ C_{41} = B_{41}C_{41}$$

and $B_{ij} = \dfrac{\xi_j - \xi_i}{\eta_j - \eta_i}$

$$E_{i,j} = x - \xi_i - B_{i,j}(y - \eta_i)$$

13

$$F_i = \tan^{-1} \frac{(B_{i,i-1} - B_{i,i+1}) Z \, d_i}{E_{i,i+1} E_{i,i-1} + (1 + B_{i,i+1} B_{i,i-1}) Z^2}$$

$$G_{ij} = \log \frac{y - \eta_j + B_{ij}(x - \xi_j) + \sqrt{1 + B_{ij}^2} \, d_j}{y - \eta_i + B_{ij}(x - \xi_i) + \sqrt{1 + B_{ij}^2} \, d_i}$$

$$d_i = \sqrt{(x - \xi_i)^2 + (y - \eta_i)^2 + Z^2}$$

Clearly, the expressions for the velocity components given above may be extended to a panel having any number of sides.

For points located at a distance from the centroid greater than four times the length of the major diagonal, the quadrilateral is approximated by a point source at the centroid. In this case, the expressions for the velocity components are considerably simplified, becoming

$$u_s = \frac{xA}{d^3} \tag{4}$$

$$v_s = \frac{yA}{d^3} \tag{5}$$

$$w_s = \frac{zA}{d^3} \tag{6}$$

where $\quad d^2 = x^2 + y^2 + z^2$

and $\quad A = $ panel area

Additional multiple expansions given in Ref. 3 for the velocity components of points located at intermediate distances from the centroid are not used in this program.

The perturbation velocity components, u_v, v_v and w_v, induced by a constant vortex distribution on the same arbitrary quadrilateral panel may be derived in a similar manner. In this case, the direction of the elementary bound vorticity must be specified in advance, and is chosen to be parallel to the panel leading edge (between corners 1 and 2).
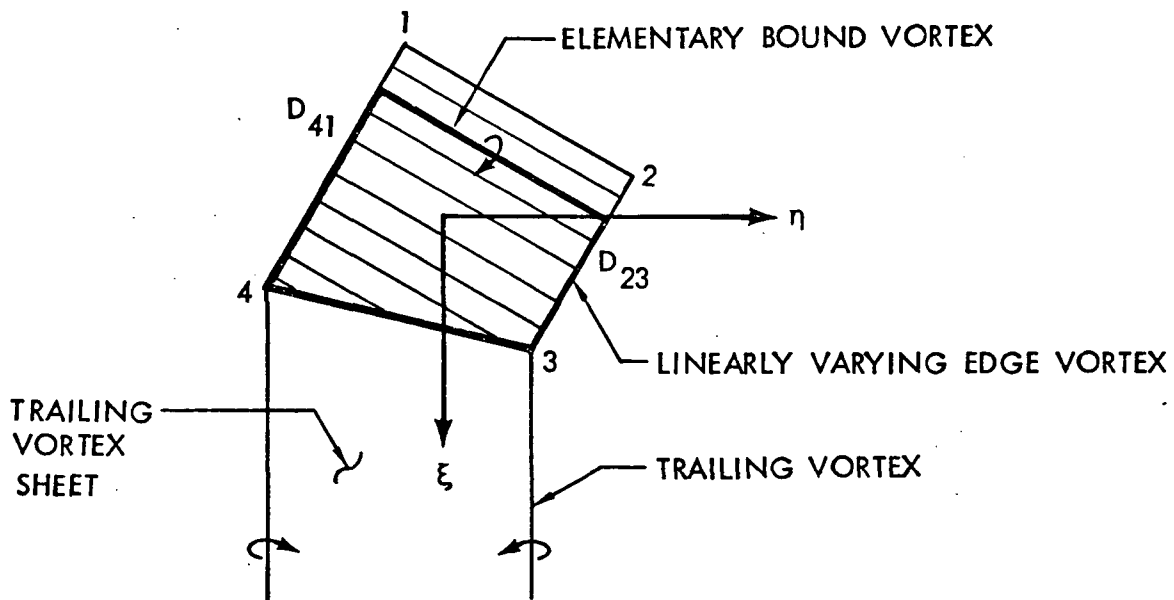

Figure 4. Vorticity Distribution

The contribution of the bound vorticity is obtained by integration (see Ref. 4). The resulting perturbation velocities at an arbitrary point, P(x,y,z) are obtained:

15

$$u_v = w_s \tag{7}$$

$$v_v = -B_{12} w_s \tag{8}$$

$$w_v = B_{12} v_s - u_s \tag{9}$$

The bound vorticity on the panel generates linearly varying vortices along the side edges 1 - 4 and 2 - 3. These edge vortices have zero strength at the leading edge, and a strength D_{ij} at the trailing edge, where $D_{ij} = \sqrt{(\xi_i - \xi_j)^2 + (\eta_i - \eta_j)^2}$. The edge vortices continue downstream from the trailing edge, maintaining a constant strength, D_{ij}. If the side edges are of unequal length, a constant vortex sheet is contained between the two trailing vortices having a net strength equal to their difference in vorticity.

Each of these edge and trailing vortices makes a contribution to the perturbation velocities. Formulas for these velocity increments are derived in Ref. 4, and tabulated in Appendix II.

Compressibility Corrections

The velocity components in compressible flow are found by applying Gothert's Rule (Ref. 5). Two options are available in the program for applying the compressibility corrections, and are designated Rule 1 and Rule 2.

Rule 1 applies the method originally proposed by Gothert.

The incompressible velocity components are calculated on an analogous body obtained by the following transformation:

16

$$x_a = x$$

$$y_a = By \qquad (10)$$

$$z_a = Bz$$

where
$$B = \sqrt{1 - M^2}$$

The boundary conditions of tangential flow are applied on the analogous body, and the resulting incompressible perturbation velocities are transformed back to the real body by

$$u = u_a/B^2$$

$$v = v_a/B \qquad (11)$$

$$w = w_a/B$$

The total velocity vector at a given point is then

$$U = U_\infty \cos \alpha \cos \beta + u$$

$$V = U_\infty \sin \beta + v \qquad (12)$$

$$W = U_\infty \sin \alpha \cos \beta + w$$

It is now known that this compressibility rule yields good results only for slender bodies at small angles of attack. The validity of this rule decreases with increasing values of the surface slope.

This effect is particularly noticeable for two-dimensional airfoil sections. In the vicinity of the nose, Gothert's Rule (which is equivalent to the Prandtl-Glauert Rule in this example) gives excessively high suction peaks on the upper surface. The reason for this failure of the theory is the manner in which the boundary conditions are satisfied at the surface of the analogous body which is thinner by the factor B than the real body, the curvature of the flow near the nose is correspondingly increased, resulting in higher suction peaks. In order to eliminate this effect, it is necessary to satisfy the boundary conditions on the surface of the real body.

Rule 2 was first proposed by Kraus in Reference 6. Beginning with the analog body as before, the expressions for the perturbation velocity components are corrected for compressibility, using Equation (11), prior to solving the boundary condition equations. The boundary conditions of tangential flow are then applied on the surface of the real body, resulting in improved results for the velocities and pressure coefficients.

The Boundary Condition Equations

The boundary condition of tangential flow at panel control points establishes a system of linear equations for determining the strengths of the source and vortex distributions. The geometrical relationship between each panel and control point is required to evaluate the coefficients of this system of equations for a given free-stream Mach number.

Normal Velocity at Panel Control Points

Each surface panel is assigned a control point located at the panel centroid. Each vortex strip is assigned a control point just behind the trailing edge of the wing in the plane of the trailing edge bisector. (This point is normally located 0.1 percent of the local chord behind the trailing edge.)

The resultant velocity normal to panel i at its control point (V_{n_i}) is the sum of the normal component of the free-stream velocity vector and the normal velocities induced by the panel source and vortex distributions. Setting the magnitude of the free-stream velocity vector equal to unity, its component normal to panel i is

$$R_i = \cos \alpha \cdot \cos \beta \cdot n_{x_i} + \sin \beta \cdot n_{y_i} + \sin \alpha \cdot \cos \beta \cdot n_{z_i} \qquad (13)$$

where n_{x_i}, n_{y_i}, and n_{z_i} are the direction cosines of the normal of panel i (see Appendix I), α is the angle of attack and β is the angle of yaw of the free-stream velocity vector in the reference axis system.

The normal component of velocity induced at the control point of panel i by the source and vortex distributions is given by

$$\begin{aligned} v_{n_i} &= \sum_{j=1}^{N} \left(n_{x_i} \cdot v_{x_{ij}} + n_{y_i} \cdot v_{y_{ij}} + n_{z_i} \cdot v_{z_{ij}} \right) \sigma_j \\ &= \sum_{j=1}^{N} a_{ij} \sigma_j \qquad (14) \end{aligned}$$

where $v_{x_{ij}}$, $v_{y_{ij}}$, and $v_{z_{ij}}$ are the three components of velocity parallel to the reference axis at control point i induced by a

unit strength source or vortex distribution on panel j, a_{ij} is the aerodynamic influence coefficient, and σ_j is the strength of the jth singularity.

The three components of velocity parallel to the reference axes are obtained by multiplying the velocity components calculated in the panel coordinate system by the transformation matrix given in Appendix I. For example,

$$V_{x_{ij}} = u_{ij} \ell_{x_{ij}} + v_{ij} \ell_{y_{ij}} + w_{ij} \ell_{z_{ij}}$$

$$V_{y_{ij}} = u_{ij} m_{x_{ij}} + v_{ij} m_{y_{ij}} + w_{ij} m_{z_{ij}}$$

(15)

$$V_{z_{ij}} = u_{ij} n_{x_{ij}} + v_{ij} n_{y_{ij}} + w_{ij} n_{z_{ij}}$$

Combining Equations (13) and (14),

$$V_{n_i} = R_i + v_{n_i}$$

(16)

$$= R_i + \sum_{j=1}^{N} a_{ij} \sigma_j$$

Solution of the Boundary Condition Equations

The boundary condition of tangential flow at panel control points is satisfied if the normal velocities are set equal to zero on all panels.

Thus

$$V_{n_i} = 0 \qquad\qquad i = 1,N$$

or

$$\sum_{j=1}^{N} a_{ij}\sigma_j = -R_i \qquad i = 1,N \qquad (17)$$

In matrix notation,

$$[A_{ij}] \{\sigma_j\} = -\{R_i\} \qquad (18)$$

where A_{ij} is the matrix of aerodynamic influence coefficients, and the right side of the equation is given by Equation (13).

This sytem of equations can be solved by direct inversion to determine the unknown source and vortex strengths. However, for the large order matrices usually encountered in aerodynamic problems, an iterative solution procedure described in Reference 7 is used.

The aerodynamic matrix is subdivided into smaller blocks, with no block exceeding order 60. The matrix elements in each block are carefully chosen to represent some well-defined feature of the configuration. For example, a wing block represents the influence of one chordwise column of wing panels, and includes the influence of the vortex strip as well as the source panels.

The initial iteration calculates the source and vortex strengths corresponding to each block in isolation. For this step, only the diagonal blocks are present in the aerodynamic matrix, and the solution is obtained by a direct inversion of the diagonal blocks. Once the initial approximation to the source and vortex

strengths is determined, the interference of each block on all the others is obtained by matrix multiplication. The incremental normal velocities obtained are subtracted from those specified on the right side of Equation (18). This process is repeated until the residual interference velocities are small enough to ensure that convergence has been achieved.

In the method of Reference 7, four optional iteration procedures are available to provide rapid convergence. These are:

1. Blocked Jacobi (JB)
2. Blocked Gauss-Seidel (GSB)
3. Blocked Successive Over-relaxation (SORB)
4. Blocked Controlled Successive Over-relaxation (CSORB)

In general, CSORB gives the most rapid convergence.

Calculation of the Pressures, Forces and Moments

Once the source and vortex strengths have been determined, the three components of velocity at control point i may be obtained.

$$u_i = \cos \alpha \cos \beta + \sum_{j=1}^{N} v_{x_{ij}} \sigma_j \tag{19}$$

$$v_i = \sin \beta + \sum_{j=1}^{N} v_{y_{ij}} \sigma_j \tag{20}$$

$$w_i = \sin \alpha \cos \beta + \sum_{j=1}^{N} v_{z_{ij}} \sigma_j \tag{21}$$

where the σ_j includes both source and vortex strengths, and

$v_{x_{ij}}$, $v_{y_{ij}}$ and $v_{z_{ij}}$ are defined following Equation (14). The pressure coefficient is calculated using the exact isentropic formula

$$C_{P_i} = -\frac{2}{\gamma M^2} \left\{ \left[1 + \frac{\gamma - 1}{2} M^2 (1 - q_i^2) \right]^{3.5} - 1 \right\} \qquad (22)$$

where
$$q_i^2 = u_i^2 + v_i^2 + w_i^2$$

For $M < .1$, the program uses the simpler formula

$$C_{P_i} = 1 - q_i^2 \qquad (23)$$

The forces and moments acting on the configuration can now be obtained by numerical integration. The normal force, side force, axial force, and pitching moments (about the origin of coordinates) of panel i are given by:

$$X_i = A_i C_{P_i} n_{x_i} \qquad (24)$$

$$Y_i = A_i C_{P_i} n_{y_i} \qquad (25)$$

$$Z_i = A_i C_{P_i} n_{z_i} \qquad (26)$$

$$M_{x_i} = Z_i Y_i - Y_i Z_i \qquad (27)$$

23

$$M_{y_i} = X_i z_i - Z_i x_i \tag{28}$$

$$M_{z_i} = Y_i x_i - X_i y_i \tag{29}$$

where A_i is the area of the panel, n_{x_i}, n_{y_i}, and n_{z_i} are the direction cosines of the normal, and x_i, y_i and z_i are the coordinates of the panel control point.

The total force and moment coefficients are obtained by summing the panel forces and moments on both sides of the plane of symmetry:

$$C_Z = \frac{1}{A_w} \sum_{i=1}^{N} Z_i \tag{30}$$

$$C_Y = \frac{1}{A_w} \sum_{i=1}^{N} Y_i \tag{31}$$

$$C_X = \frac{1}{A_w} \sum_{i=1}^{N} X_i \tag{32}$$

$$C_{M_z} = \frac{1}{A_w \bar{c}} \sum_{i=1}^{N} M_{z_i} \tag{33}$$

$$C_{M_y} = \frac{1}{A_w \bar{c}} \sum_{i=1}^{N} M_{y_i} \tag{34}$$

$$C_{M_X} = \frac{1}{A_w \bar{c}} \sum_{i=1}^{N} M_{x_i} \qquad (35)$$

Finally, the lift, side force and drag coefficients are:

$$C_L = C_Z \cos \alpha - (C_X \cos \beta - C_Y \sin \beta) \sin \alpha \qquad (36)$$

$$C_S = C_Y \cos \beta + C_X \sin \beta \qquad (37)$$

$$C_D = (C_X \cos \beta - C_Y \sin \beta) \cos \alpha + C_Z \sin \alpha \qquad (38)$$

The program computes the forces and moments acting on the wing, and sums them to obtain the total forces and moments on the complete configuration. Wing section forces and moments may also be calculated at the user's option.

Relaxed Wake Model

In the analysis of configurations with high circulation, the orientation of the trailing vortex sheet can have an important effect on the calculated results, particularly in the case of multiple components, e.g., a wing with slotted flap or wing with tailplane. The trailing vortex sheet should, in fact, carry no load, but, satisfying this condition renders the problem non-linear insofar as the pressure distribution and the wake shape are interdependent. Analysis of such problems, therefore, requires an iterative procedure in which the wake shape is first assumed in order to solve for the pressure distribution; knowledge of the pressure distribution allows the streamlines to be calculated, which give the force-free orientation of the trailing vortex sheet. Further iterations may be necessary to make the pressure distribution and wake shape compatible.

In the present method, the wake model and iterative technique are similar to those used in a quadrilateral vortex-lattice method (Ref. 8). The trailing vortex sheet is represented by a system of discrete vortices (Figure 5) attached to the panel edges at the trailing-edge of each component (i.e., wing, flap, etc.). Each vortex is segmented over the region from its starting point to a station a short distance downstream of the last component. The segment lengths in this region can be varied from vortex to vortex so that small segments can be used where the vortices are expected to bend most, and larger segments can be used where little displacement is expected. This helps to minimize computing time. Downstream of the segmented region, each vortex is straight, semi-infinite and streamwise. Initially, all the vortices are assumed straight in the streamwise direction. In the iterative procedure, each vortex segment is aligned with the local mean velocity --
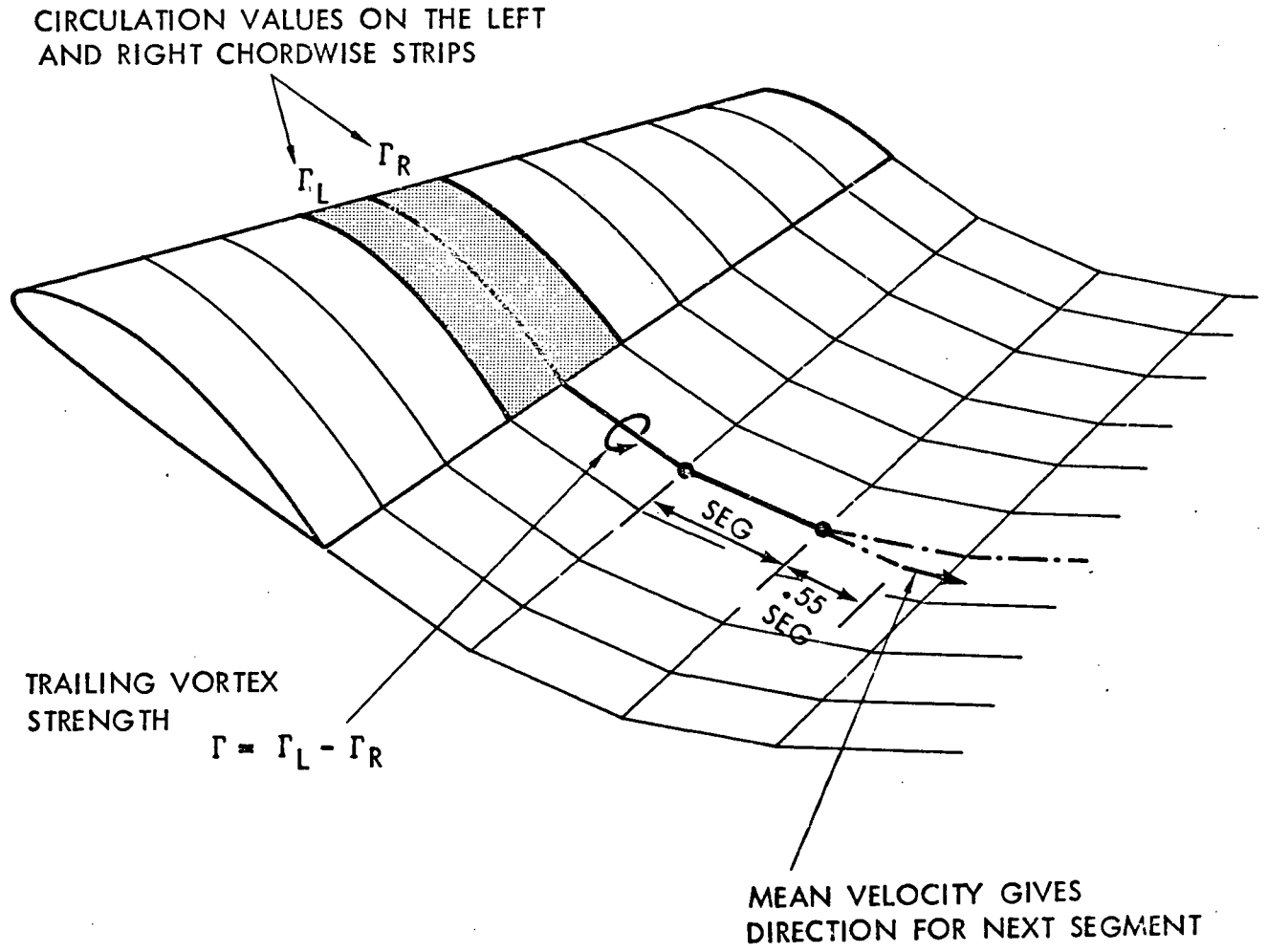
CIRCULATION VALUES ON THE LEFT
AND RIGHT CHORDWISE STRIPS

Γ_R

Γ_L

SEG

.55
SEG

TRAILING VORTEX
STRENGTH

$\Gamma = \Gamma_L - \Gamma_R$

MEAN VELOCITY GIVES
DIRECTION FOR NEXT SEGMENT

Figure 5.   Trailing Vortex Segments

27

calculated near the segment mid point, Reference 8, Figure 5 - to
render the segment approximately force free. But, the spanwise
movement of the vortices is not allowed in the present program;
this restriction is necessary at this time to avoid spurious re-
sults when the discrete trailing vortices from one component pass
close to the surface control points on another surface. Canceling
the spanwise movement of the vortices maintains the correct rela-
tionships between the discrete vortices and the control points.
This is a near-field problem associated mainly with discrete vor-
tex models, and is particularly apparent in close-approach situa-
tions such as when the wing wake passes over a slotted flap. How-
ever, techniques such as those of Refs. 9 and 10 can remove this
restriction to allow a complete wake roll-up calculation.

The strength of each trailing vortex is the difference in
circulation between the two chordwise panel strips adjacent to the
start of the vortex (Figure 5). The strengths are changed at
each iteration (Figure 6). To minimize the computation in each
iteration, the influence coefficient matrices for the wake vor-
tices are stored separately. Clearly, the surface panel influence
coefficients remain constant as the wake shape changes; only the
wake contributions need be recalculated in each iteration. Stor-
ing the wake influence coefficients separately allows the new set
to be compared with the previous set; then only the differences
are added to the main influence coefficient matrices.

The number of iterations for wake shape is an input parameter
at this stage. The first iteration gives most of the non-linear
effect, and is probably as far as the calculation need be taken
with the present restriction of canceling the spanwise movement.
This model should be adequate up to C_L values of the order of 2.

Higher lift values, and also more detailed evaluation of pres-
sures such as in the tip-edge vortex region, will require the
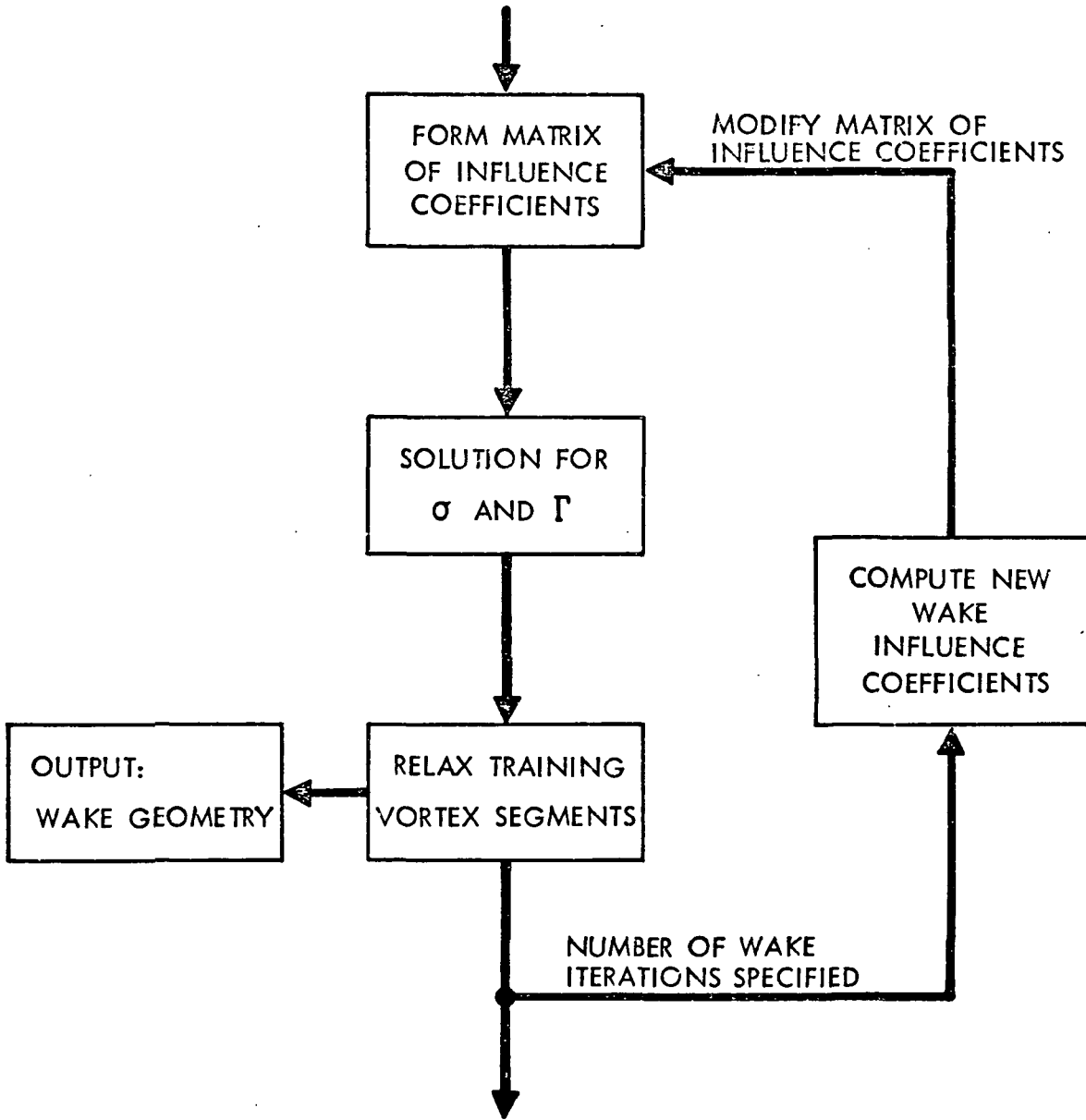
28

Figure 6. Wake Iteration Procedure

complete roll-up calculation and more iterations. In this case, a convergence criterion would be required to control the number of iterations. This criterion could be based on the changes in wake influence coefficients or on some overall parameter such as C_L.

BOUNDARY LAYER CALCULATION METHODS

The _finite_ span multi-element wing is divided into a number of streamwise strips. Each strip is treated as if it were a separate _infinite_ span wing. On each strip the boundary layer development is calculated along stream lines from the stagnation line to the trailing edge of each element using the boundary layer methods currently in Program VIP (Ref. 1). No major modification of the boundary layer programs has been made. At the current state of development of three-dimensional analyses for high-lift systems, it is believed that the infinite span boundary layer methods adequately predict the boundary layer development. At high angles-of-attack, or with very low aspect ratios the infinite-span methods are not expected to accurately predict the boundary layer development, particularly in the wing tip region. However, other phenomena, such as tip vortex formation, wake roll-up and main wing vortex wake-flap interaction greatly influence the inviscid flow, and must be taken into account before fully three-dimensional boundary layer methods are considered.

The boundary layer methods are described in detail in Reference 1, and are summarized briefly in the following paragraphs.

Stagnation Line Flow

Theoretical predictions of the stagnation line flow of an infinite yawed wing by Cumpsty and Head (Ref. 11) and Bradshaw (Ref. 12) as well as others indicate that the boundary layer approaches an asymptotic state where frictional forces are balanced by divergence of the flow from the spanwise to the streamwise direction. Cumpsty and Head found that the stagnation line boundary layer integral parameters (H, θ, and C_f) and the state (laminar

31

or turbulent) correlate with the parameter $C* = V^2/(\nu \frac{dU}{ds})$.

Cumpsty and Head (Ref. 13) later experimentally verified their theoretical correlations, and it is these correlations that are used to determine the boundary layer characteristics on each element of the swept finite wing. If the wing is unswept, then conventional two-dimensional correlations are used to start the boundary layer calculations.

Conventional Boundary Layer Methods

Integral boundary layer methods are used for all conventional boundary layers such as on the upper and lower surfaces of the main element, the lower surfaces of flap elements and the upper surfaces of flap elements up to the slot exits. If the Reynolds number is sufficiently low to allow laminar flow on a swept wing, the two-dimensional equations of Curle (Ref. 14) are solved along external streamlines to determine the laminar boundary layer development. It is assumed that laminar cross-flow effects have a negligible influence on the overall calculation, at least for moderate sweep angles.

The streamwise boundary layer characteristics are used with the correlation of Smith (Ref. 15) to determine the point of laminar instability. With the point of instability, the momentum thickness Reynolds number distribution, R_θ, and the pressure gradient parameter, $\bar{k}$, known, the transition point is determined using Granville's correlation (Ref. 16). The turbulent boundary layer development over an infinite swept wing is calculated using the method of Cumpsty and Head (Ref. 17). If the initial stagnation line flow is turbulent, Cumpsty and Head's method is used from the stagnation line to the element trailing edge.

32

In those cases where laminar separation occurs prior to transition, a correlation based on the data of Gaster (Ref. 18) is used to determine if turbulent reattachment occurs. Should reattachment be predicted, the calculation continues for turbulent flow; if catastrophic separation is predicted, the boundary layer calculation is terminated.

Confluent Boundary Layer Method

The boundary layer development from the slot exit to the trailing edge of each flap upper surface is determined using an infinite swept wing version of a finite difference method developed by Dvorak (Ref. 19). This method treats the upstream element wake and flap boundary layer as if it were all one thick boundary layer with initially an embedded potential core. The differencing scheme is based on the method of Crank and Nicholson (Ref. 20), as modified by Dvorak and Head (Ref. 21). The turbulent closure is via an eddy viscosity model modified for the confluent boundary layer from the two-dimensional model for boundary layers and wall jets developed by Dvorak (Ref. 19). The calculations include the effects of longitudinal surface curvature and the variation of static pressure through the boundary layer. The static pressure field, $p(s,z)$, is determined directly from the potential flow solution.

The initial velocity profile required to start the finite difference calculation at the slot exit is constructed from: (1) the integral boundary layer solution at the slot exit on the upper surface of the component in question; (2) the potential core as determined from the potential flow solution; and (3) the upper and lower surface boundary layer solutions at the trailing edge of the upstream element. With the initial velocity profile

the surface curvature and the static pressure field known, the
boundary layer equations are solved in a forward marching fashion
to the trailing-edge of the component.

VISCOUS/INVISCID INTERACTION

The effect of boundary layer displacement on the potential
flow is simulated by distributing sources of known strength on
the panels used to describe the wing geometry. The strengths of
these sources are determined directly from the boundary layer
solutions as $q_i = \frac{d}{ds} (U_i \delta_i^*)$ where U_i is the streamwise potential
flow velocity at the edge of the boundary layer and δ_i^* is the
streamwise displacement thickness.

The addition of this source distribution modifies the normal
velocity at the control point of panel i. Consequently, the bound-
ary condition (Equation 16) is modified as follows

$$V_{ni} = R_i + q_i + \sum_{j=1}^{N} a_{ij} \sigma_j \tag{39}$$

Since q_i is known for each iteration, the right hand side only of
Equation 18 is altered, giving (in matrix notation)

$$\left[A_{ij} \right] \sigma_j = - R_i - q_i \tag{40}$$

Because the original geometry is not modified by the use of
distributed sources, the aerodynamic influence coefficient matrix
need not be recalculated. Subsequent iterations between the po-
tential flow and boundary layer calculations results in convergent

solutions. The alternative procedure, that is, modifying the geometry directly by addition of the displacement thickness, while quite widely used in two dimensions, becomes untenable in three dimensions. Primarily, this is a result of having to calculate and invert a new aerodynamic influence coefficient metrix at each iteration due to the change in geometry. Without considering the additional cost of smoothing the geometry and redefining the panels at each iteration, the additional cost of calculating and inverting the influence coefficient matrix at each iteration can be seen from the following illustration.

<u>Wing</u>: Kolbe and Boltz (Ref. <u>22</u>)
   -- sweep angle 45°
   -- taper ratio .5
   -- aspect ratio 3
   -- number of panels 510
   -- computer CDC 7600

Calculation and inversion of the aerodynamic influence coefficient matrix required 193 CP seconds on the CDC 7600. The iterative solution required 2.1 CP seconds. Subsequent iterations with the source method requried only the 2.1 CP seconds per iteration to obtain a new potential flow solution, with convergence acheieved in 4 iterations. The direct displacement thickness method would have required as a minimum an additional 193 CP seconds per iteration to obtain the desired solution. Assuming that it would also have converged in 4 iterations, an additional (193 x 3) = 579 CP seconds would have been needed to complete the viscous/inviscid calculation. On slower computers, the additonal time requirements would be prohibitive.

CALCULATION PROCEDURE

The computer program is made up of a series of overlays, as shown in Figure 7. The executive program, VIP3D, controls the overall analysis by calling in turn the overlays containing the potential flow and boundary layer calculation methods. The calculation sequence is outlined as follows.

i) The input geometry, as represented by a series of streamwise planar panels is lofted in Program WBPAN.

ii) The potential flow pressure field is computed for the multi-element configuration in Program WBAERO. Off-body pressures over flap upper surfaces are computed as part of the analysis. Included in the calculation is the force-free wake analysis. The multi-element wing can consist of up to four elements, a leading-edge slat, the main wing and double slotted flaps.

iii) The boundary layer development is determined for each streamwise strip beginning inboard and proceeding spanwise to the wing tip. Each strip is treated as a separate infinite yawed wing. The laminar and turbulent boundary layer developments are determined for each element of the strip as a function of the potential flow pressure distribution. Transition or laminar separation and turbulent separation are predicted, if present. Program IBL is used for the integral boundary layer analysis, and Program INSPAN, the finite difference method, is used when flap upper surfaces are considered.

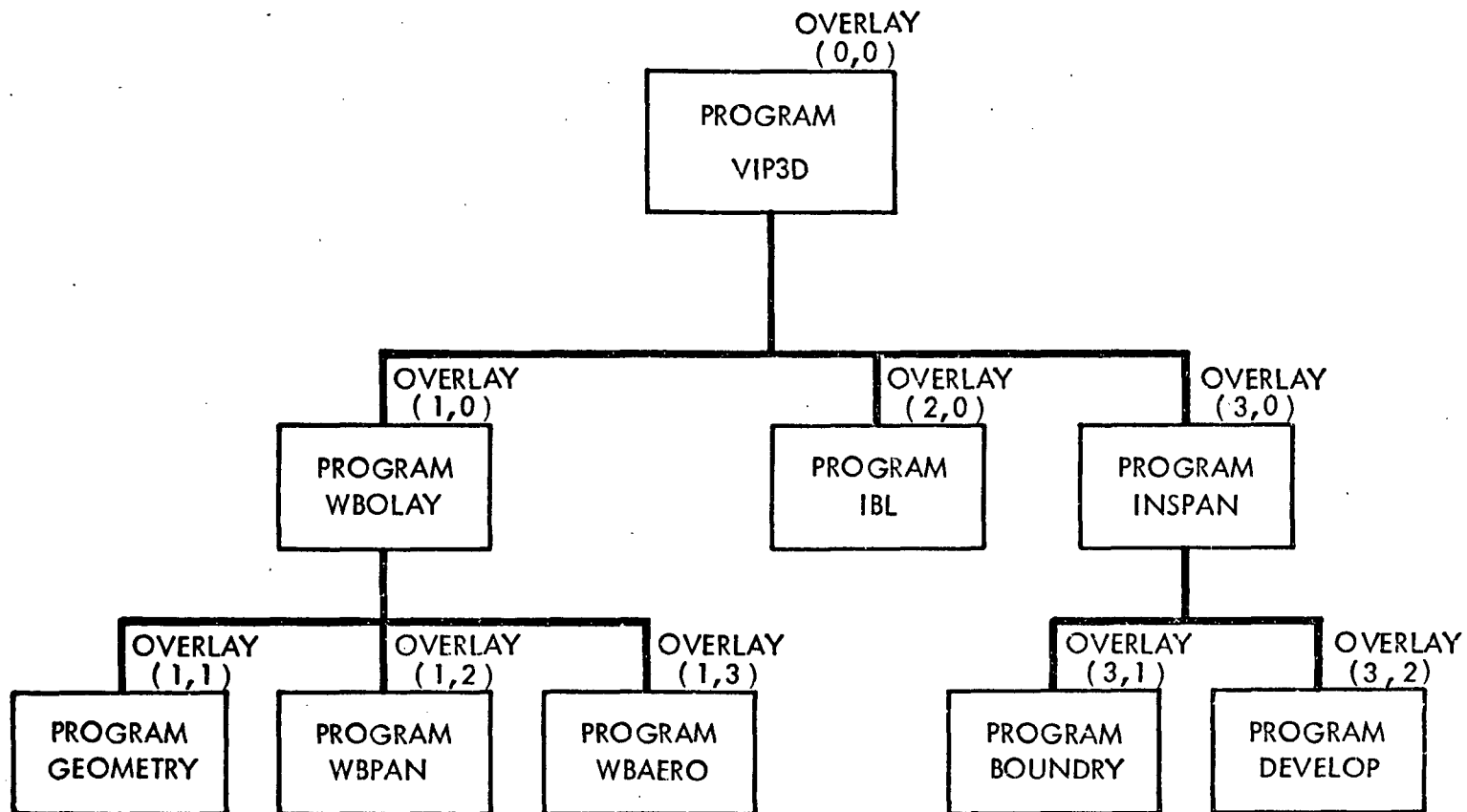iv) Source distributions representing the boundary layer displacement effect are determined for each streamwise strip.

Figure 7. Viscous/Potential Flow Program Overlay Structure

37

v) A new potential flow solution is computed taking into account the source distribution computed in step (iv).

Steps (iii) through (v) are repeated until convergence (based on configuration lift coefficient) is achieved. Forces and moments are then calculated, both for the complete configuration, and for the individual sections. The calculation procedure is illustrated in Figure 8 .
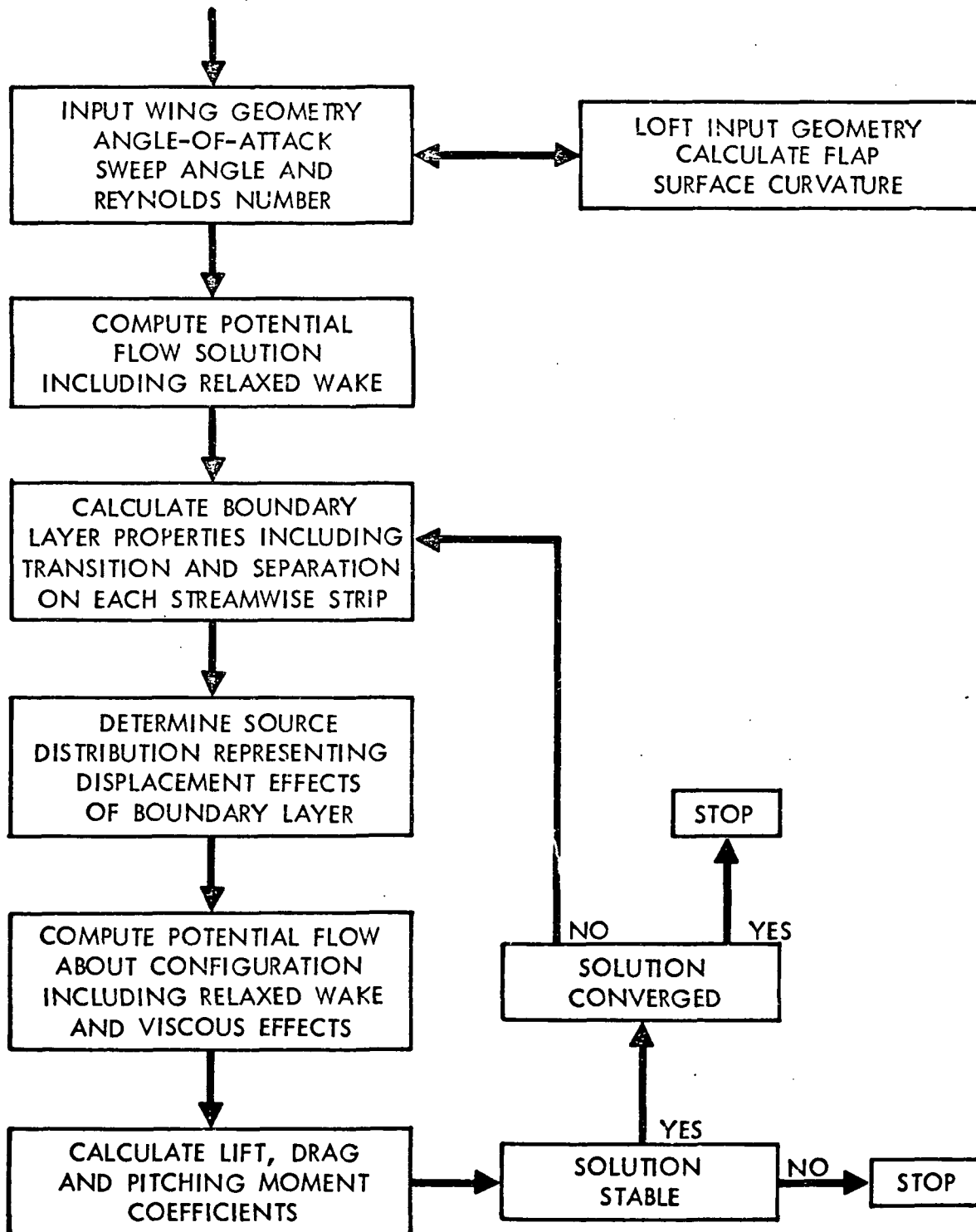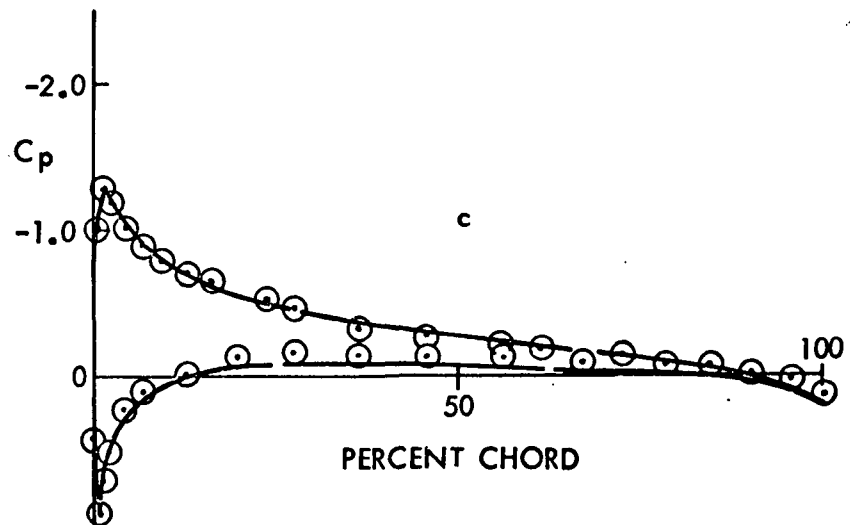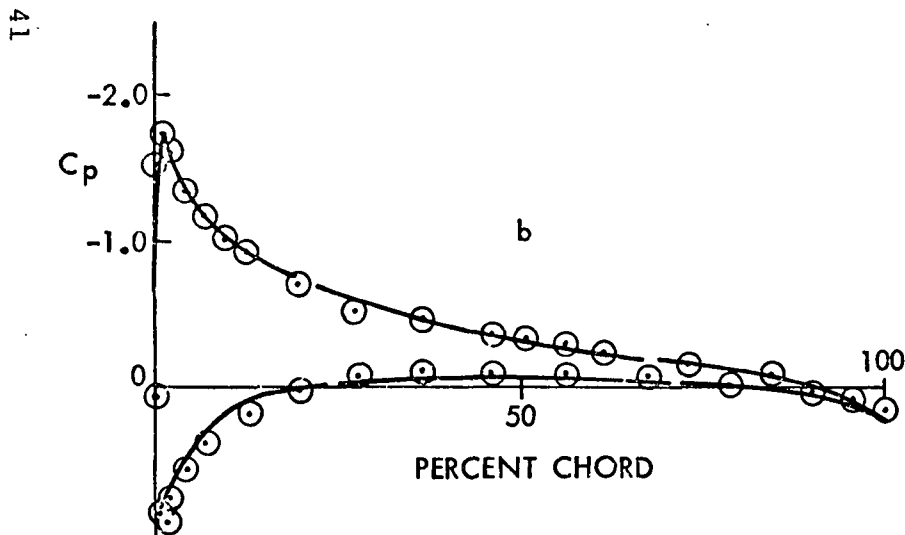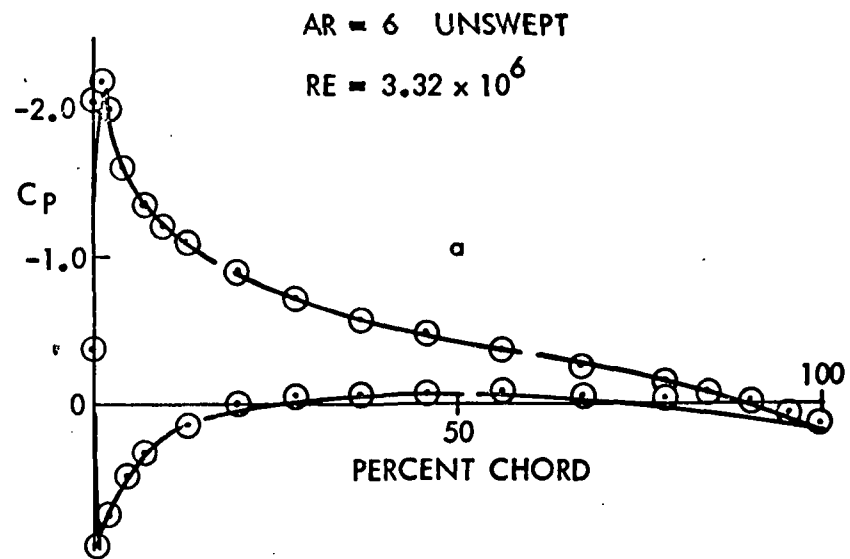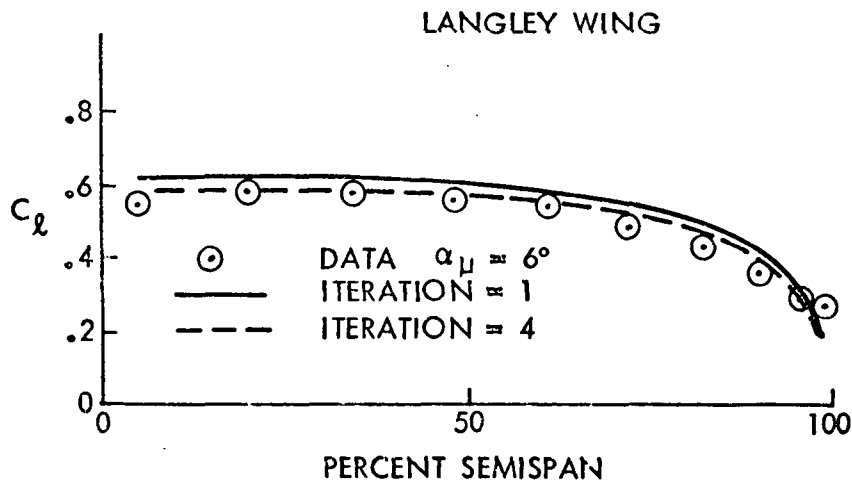
Figure 8. Computation Procedures

CALCULATIONS AND DISCUSSION OF RESULTS

Calculations have been made to compare with experimental results available from a recent NASA Langley Research Center study. The experimental configuration consisted of a rectangular wing of aspect ratio = 6 mounted on a splitter plate in the wind tunnel. A range of angles of attack were investigated for a series of sweep angles. Calculations made for the zero sweep case are shown in Figure 9. Comparisons with experiment show some improvement in the predicted spanwise load distribution with viscous effects added. Predicted streamwise pressure distributions (fourth iteration) at three spanwise locations are in good agreement with experiment. Tip-edge vortex formation and wake roll-up are not modelled in this calculation, although at the angle of attack considered (6^0) their effect would be small. There is, however, already some modification to the experimental pressure distribution at the 98.8% semispan location due to the tip-edge vortex at $\alpha = 6^0$. The boundary layer calculations were based on forced transition at 10% chord on the wing to correspond to a transition strip at 5% chord on both upper and lower surfaces of the wing in the experimental case.

A second configuration investigated was the swept wing case of Kolbe and Boltz (Ref. 22). This case is of interest because of the low aspect ratio (3), the sweep angle (45^0) and the taper ratio (.5). Several investigatators have used the experimental data to compare with their calculation methods. Of particular interest are the studies by Hess (Ref. 23). His inviscid calculations indicated a spanwise load distribution approximately 15% higher than experiment. He postulated that the difference was due to viscous effects, and attempted to prove it by, in his own words, adding a crude estimate of displacement thickness to the

LANGLEY WING

AR = 6   UNSWEPT

RE = 3.32 x 10^6

C_ℓ

.8

.6

.4

.2

0

⊙   DATA α_μ = 6°

———   ITERATION = 1

- - - -   ITERATION = 4

0   50   100

PERCENT SEMISPAN

C_P

-2.0

-1.0

0

a

50   100

PERCENT CHORD

41

C_P

-2.0

-1.0

0

b

50   100

PERCENT CHORD

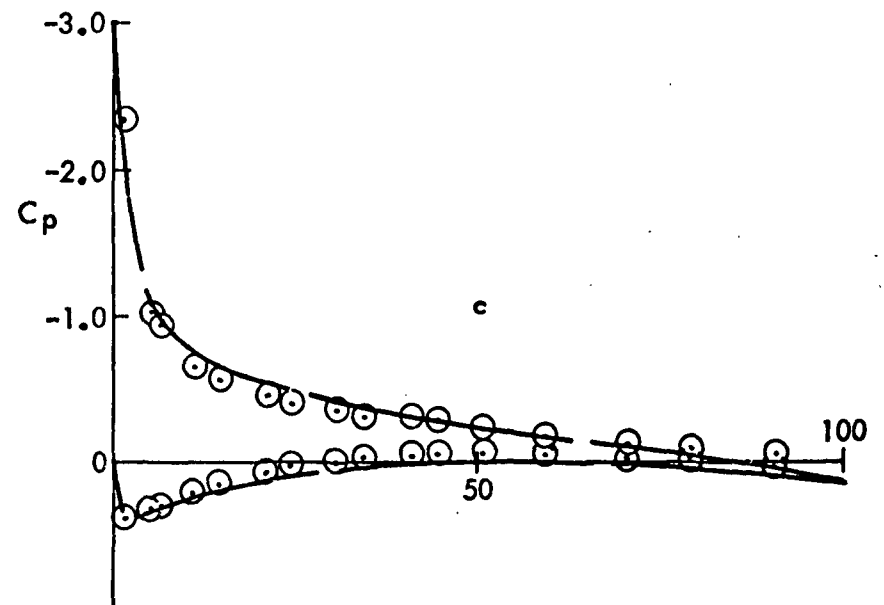C_P

-2.0

-1.0

0

c

50   100
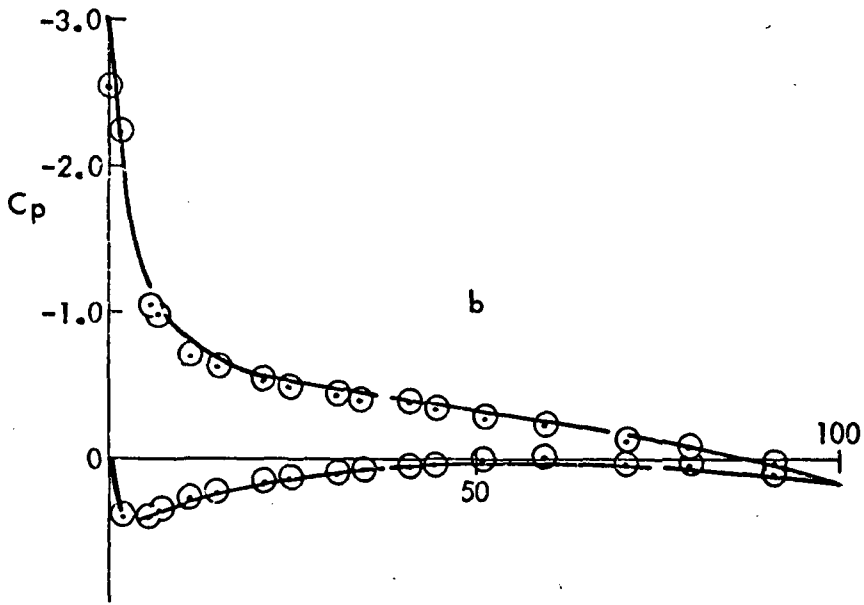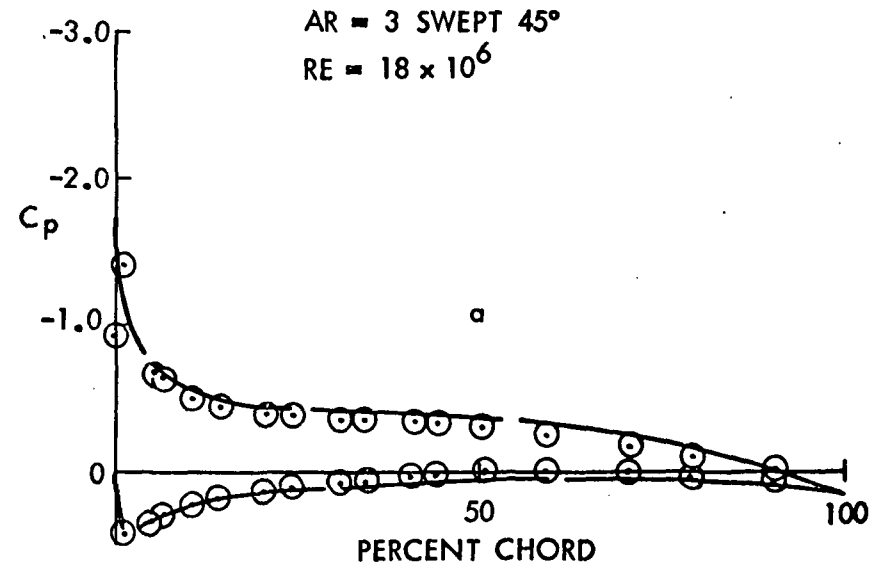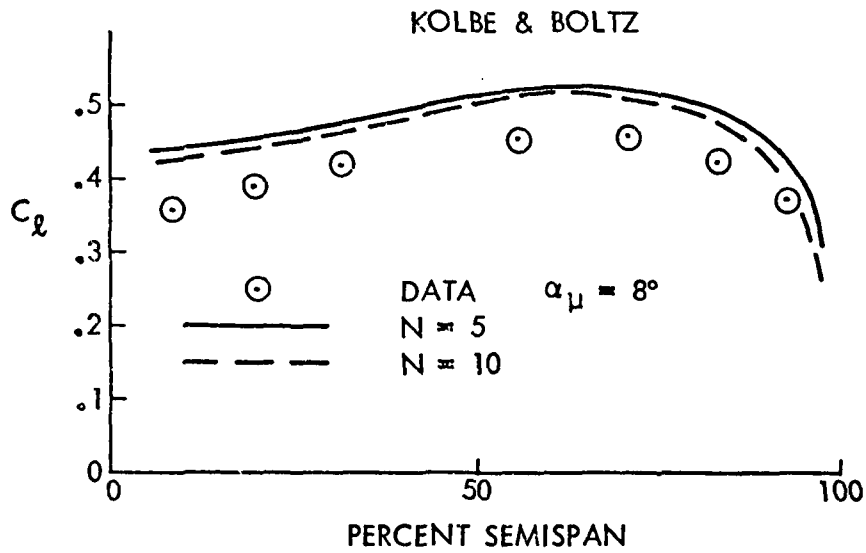
PERCENT CHORD

a) 34.4%,   b) 81.9%,   c) 95.4% SEMISPAN

Figure 9.   Comparison of Measured and Predicted Spanwise Loading and
Pressure Distributions

wing. The new calculations were in much closer agreement with experiment, and according to Hess, justified his assumption. Calculations by the present method, however, dispute this assumption. As shown in Figure 10, the inviscid calculation also is high by about 15% in spanwise loading, with only modest improvement when the number of spanwise strips used to model the wing is doubled. At the Reynolds number of the test, 18 million, the calculations indicate that the viscous interaction with the pressure field is quite small, smaller in fact than the difference between calculations using 5 and 10 spanwise strips. Because of the high Reynolds number and the symmetric, relatively thin airfoil section (7.6% t/c on sections parallel to the plane of symmetry) and the low angle of attack ($\alpha = 8^0$), viscous effects should be small. Therefore some other hypothesis is needed to explain the differences between theory and experiment. The explanation appears to come from the shape of the wing tip (rounded in the case of Kolbe and Boltz) and from the low aspect ratio. Experimental evidence collated by Hoerner (Ref. 24) shows that rounding tip edges (lateral and streamwise) reduces the effective aspect ratio and the lift curve slope of the wing. As geometric aspect ratio decreases, the influence of rounding becomes more and more predominant. Since the inviscid calculation methods (Hess and the present method) do not specifically take into account the tip-edge shape, they will likely over-predict the lift distribution.

A simple calculation substantiates this assumption. Sharp lateral-edge wings with an aspect ratio of 3 have a lift curve slope, $dC_L/d\alpha^0 \simeq .058$, whereas with rounded edges, $dC_L/d\alpha^0 \simeq .05$ (Ref. 24). The difference in C_L for wings having symmetric sections at 8^0 angle-of-attack is approximately .065, or very close to the difference between theory and experiment shown in Figure 10.

a) 19.5 %, b) 70.7 %, c) 92.5 % SEMISPAN

Figure 10. Comparison of Measured and Predicted Spanwise Loading and Pressure Distributions

43

It would appear that in order to obtain improved results for low aspect ratio wings, the potential flow methods must use more realistic paneling in the tip region, and, perhaps even incorporate tip-edge vortex roll-up model.

The multi-element capability of the program was checked using a wing configuration that has been tested in the Ames 40- by 80-foot Wind Tunnel (Ref. 2). The wing, consisting of the RAE 2815 airfoil and single slotted flap cross-section had a span of 52.6 feet, and a reference chord of 5.58 feet, giving an aspect ratio of 9.43. The calculations were performed using 68 chordwise panels and 3 streamwise strips to represent the wing on one side of the plane of symmetry. This is a rather coarse paneling, but it should demonstrate the trends. The calculations for lift, drag and pitching moment coefficients for a series of angles-of-attack are shown in Figure 11. The spanwise distributions of lift, drag and pitching moment are shown in Figure 12. The calculations which include viscous effects are determined from the third iteration through the program. A second calculation was made with the wing and flap wakes allowed to relax in a plane parallel to the plane of symmetry. This resulted in a slightly reduced lift coefficient as indicated in Figure 11. Further work will include detailed comparisons between the predictions of this theoretical method and the data from the Ames experimental program.
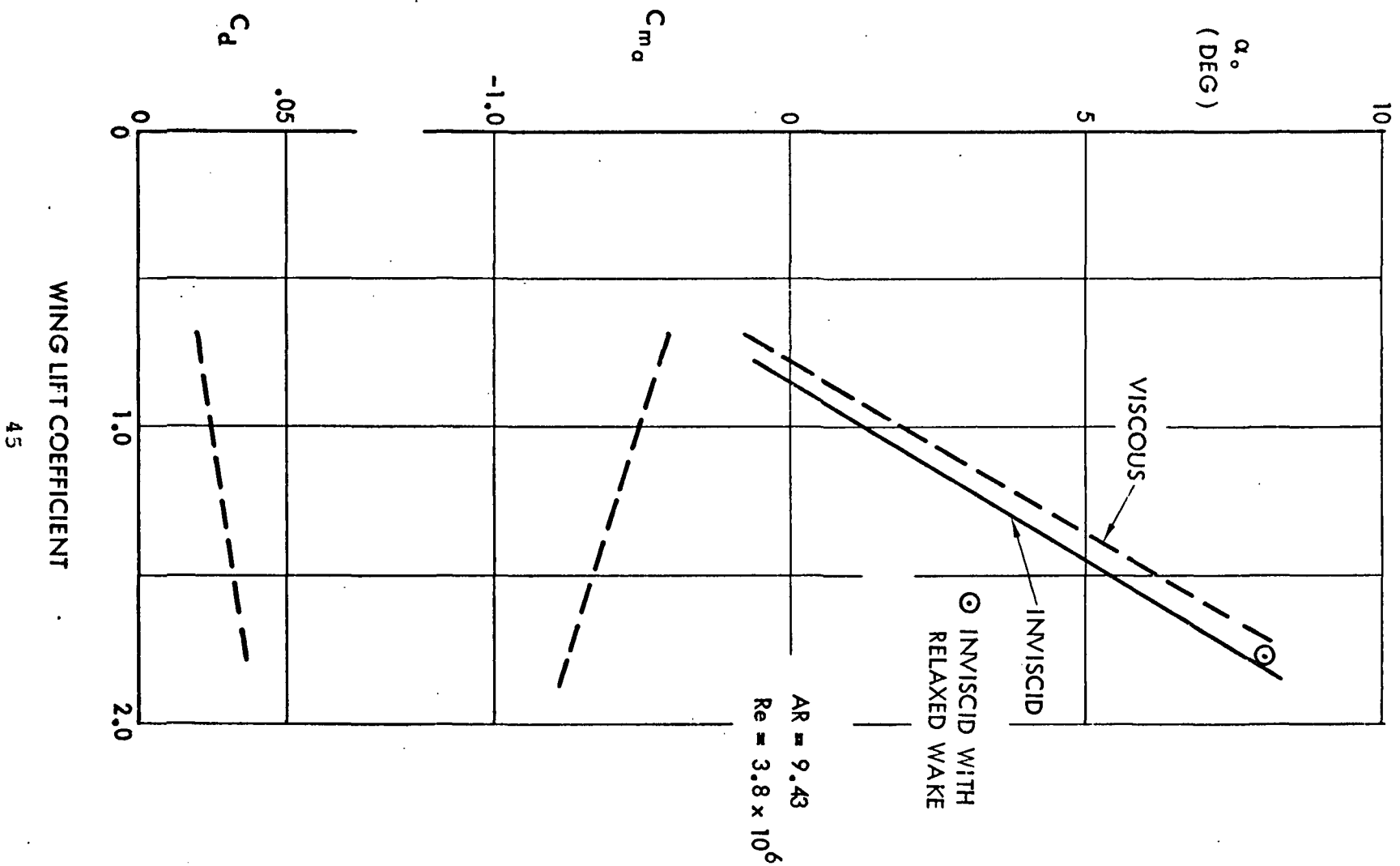
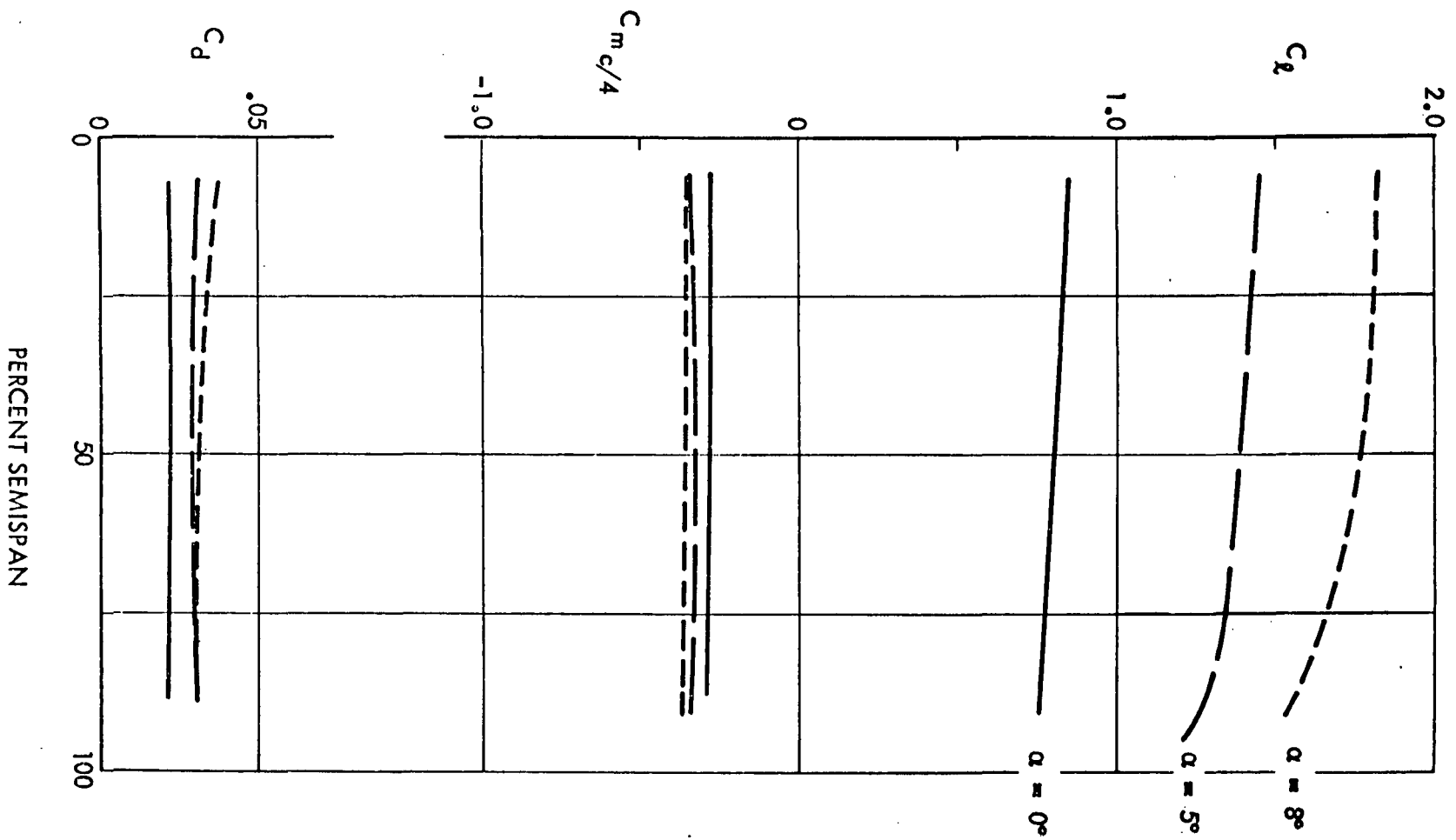Figure 11. Predicted Lift, Drag and Pitching Moment Coefficients for an RAE 2815 Wing with Single Slotted Flap

Figure 12. Predicted Spanwise Distributions of Lift, Drag and Pitching Moment for an RAE 2815 Wing with Single Slotted Flap.

CONCLUSIONS AND RECOMMENDATIONS

The three-dimensional viscous/potential flow interaction analysis program described in this report is currently the only one of its kind. Its present capability includes the analysis of multi-element wings having full span slats and slotted flaps. A force-free (relaxed) wake model is included in order to improve the prediction of surface pressures on the individual wing components. Wake roll-up and tip-edge vortex roll-up are not yet modeled, but will be required in the future if partial span slats or flaps are to be considered.

The method in its present form has been compared with only a very small data set; however, the various programs which make up the complete program have been used independently or in combination with other programs for some time. In general, the methods are stable and have demonstrated good agreement with experiment over a wide range of applications. It is concluded that the present program will also prove to be very useful over a wide range of three-dimensional wing applications.

A specific conclusion can be drawn in regards to the use of sources to represent the displacement effect of the boundary layer on the potential flow. In three dimensions, the computational superiority of this approach is clearly what makes such a calculation procedure practical. The direct addition of displacement thickness with the accompanying necessity to distribute and smooth the new surface, and subsequently reinvert the aerodynamic influence matrix at each iteration is almost prohibitive of computer time.

It is recommended that once the close-approach problem of a vortex wake interacting with the vortex elements of a downstream

47

surface is solved, the calculation procedure be expanded to include
models for complete wake roll-up and tip-edge vortex roll-up.

48

REFERENCES

1. Dvorak, F.A. and Woodward, F.A., "A Viscous/Potential Flow Interaction Analysis Method for Multi-Element Infinite Swept Wings: Volume I", NASA CR-2476, November 1974.

2. Olson, L.E. and Dvorak, F.A., "Viscous/Potential Flow About Multi-Element Two-Dimensional and Infinite-Span Swept Wings: Theory and Experiment", AIAA 14th Aerospace Sciences Meeting, Washington, D.C., January 1976.

3. Hess, J.L. and Smith, A.M.O., "Calculation of Potential Flow about Arbitrary Bodies", Progress in Aeronautical Sciences, Vol. 8, Pergamon Press, 1967.

4. Woodward, F.A., "An Improved Method for the Aerodynamic Analysis of Wing-Body-Tail Configurations in Subsonic and Supersonic Flow: Part I: Theory and Application", NASA CR-2228, May 1973.

5. Gothert, B., "Plane and Three-Dimensional Flow at High Subsonic Speeds", NACA TM 1105, 1946.

6. Kraus, W. and Sacher, P., Das MBB Unterschall Panel Verfahren: Dreidimensionale Potentialtheorie bei beliebig Vorgegebener Mehr Korperanordnung", MBB Report UFE-672-70(0), December 1970.

7. Bratkovich, A. and Marshall, F.J., "Iterative Techniques for the Solution of Large Linear Systems in Computational Aerodynamics", J. Aircraft, Vol. 12, No. 2, February 1975.

8. Maskew, B., "Numerical Lifting Surface Methods for Calculating the Potential Flow about Wings and Wing-Bodies of Arbitrary Geometry", Ph.D. Thesis, Loughborough Univ. of Tech., England, October 1972.

9. Maskew, B., "A Subvortex Techniuqe for the Close Approach to a Discretized Vortex Sheet", NASA TM X 62,487, September 1975.

10. Maskew, B., "A Submerged Singularity Method for Calculating Potential Flow Velocities at Arbitrary Near-Field Points", NASA TM X-73, 115, March 1976.

11. Cumpsty, N.A. and Head, M.R., "The Calculation of Three-Dimensional Turbulent Boundary Layers, Part II: Attachment - Line

11. Flow on an Infinite Swept Wing", Aero. Quart., Vol. XVIII, May 1967.

12. Bradshaw, P., "Calculation of Three-Dimensional Turbulent Boundary Layers", J. Fluid Mech., Vol. 46, 1971.

13. Cumpsty, N.A. and Head, M.R., "The Calculation of the Three-Dimensional Turbulent Boundary Layer, Part III: Comparison of Attachment - Line Calculations with Experiment", Aero. Quart., Vol. XX, May 1969.

14. Curle, H., "A Two-Parameter Method for Calculating the Two-Dimensional Incompressible Laminar Boundary Layer", J.R. Aero. Soc., Vol. 71, 1967.

15. Smith, A.M.O., "Transition, Pressure Gradient and Stability Theory", Proc. 9th Internat. Congress of Appl. Mach., Brussels, Vol. 7, 1957.

16. Granville, P.S., "The Calculation of the Viscous Drag of Bodies of Revolution", David W. Taylor Model Basin Report 849, 1953.

17. Cumpsty, N.A. and Head, M.R., "The Calculation of Three-Dimensional Turbulent Boundary Layers, Part I: Flow Over the Rear of an Infinite Swept Wing", Aero. Quart., Vol. XVIII, February 1967.

18. Gaster, M., "The Structure and Behavior of Laminar Separation Bubbles", ARC 28-226, 1967.

19. Dvorak, F.A., "Calculation of Turbulent Boundary Layers and Wall Jets over Curved Surfaces", AIAA Journal, Vol. 11, No. 4, April 1973.

20. Crank, J. and Nicholson, P., "A Practical Method for Numerical Evaluation of Solutions of Partial Differential Equations of the Heat Conduction Type", Proc. Cambridge Phil. Soc., 43, 1947.

21. Dvorak, F.A. and Head, M.R., "Heat Transfer in the Constant Property Turbulent Boudnary Layer", Int. J. Heat Mass Transfer, Vol. 10, 1967.

22. Kolbe, C.D. and Boltz, F.W., "The Forces and Pressure Distribution at Subsonic Speeds on a Plane Wing Having 45° of

22.   Sweepback, an Aspect Ratio of 3 and a Taper Ratio of 0.5",
       NACA RM A51G31, October 1951.

23. Hess, J.L., "Calculation of Potential Flow About Arbitrary
       Three-Dimensional Lifting Bodies", Report No. MDC J 5679-01,
       Douglas Aircraft Company, October 1972.

24. Hoerner, S.F. and Borst, H.V., Fluid-Dynamic Lift, Hoerner
       Fluid Dynamics, Brick Town, N.J., 1975.

APPENDIX I

PANEL GEOMETRY CALCULATION PROCEDURE

The analytical procedure presented here follows closely the method first developed in Reference 14. A quadrilateral surface element is described by four corner points, not nesessarily lying in the same plane, as shown in the sketch. Note that the numbering convention of the corner points differs from that used in the preceding text. The quadrilateral element is approximated by a planar panel as follows:
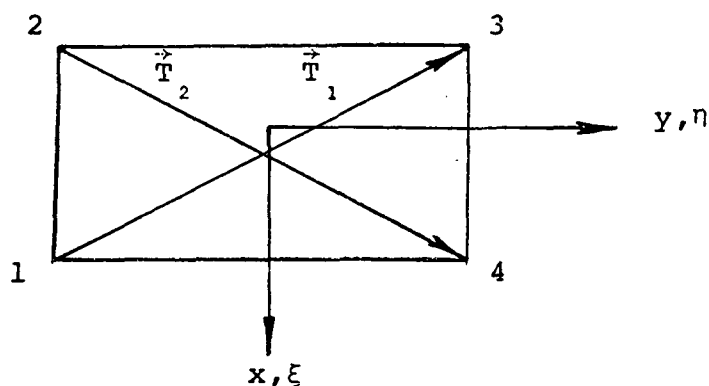
The coordinates in the reference coordinate system are identified by their subscripts. The components of the diagonal vectors $\vec{T}_1$ and $\vec{T}_2$ are

$$T_{1x} = x_3 - x_1 \qquad T_{1y} = y_3 - y_1 \qquad T_{1z} = z_3 - z_1$$

$$T_{2x} = x_4 - x_2 \qquad T_{2y} = y_4 - y_2 \qquad T_{2z} = z_4 - z_2$$

We may now obtain a vector $\vec{N}$ (and its components) by taking the cross product of the diagonal vectors.

$$\vec{N} = \vec{T}_2 \times \vec{T}_1$$

$$N_x = T_{2y}T_{1z} - T_{1y}T_{2z}$$

$$N_y = T_{1x}T_{2z} - T_{2x}T_{1z}$$

$$N_z = T_{2x}T_{1y} - T_{1x}T_{2y}$$

The unit normal vector, $\vec{n}$, to the plane of the element is taken as $\vec{N}$ divided by its own length, N (direction cosines of outward unit normal).

$$n_x = \frac{N_x}{N}$$

$$n_y = \frac{N_y}{N}$$

$$n_z = \frac{N_z}{N}$$

where $N = \left[N_x^2 + N_y^2 + N_z^2 \right]^{\frac{1}{2}}$

The plane of the element is now completely determined if a point in this plane is specified. This point is taken as the point whose coordinates, $\bar{x}$, $\bar{y}$, $\bar{z}$, are the averages of the coordinates of the four input points.

53

$$\bar{x} = \frac{1}{4} \left[x_1 + x_2 + x_3 + x_4 \right]$$

$$\bar{y} = \frac{1}{4} \left[y_1 + y_2 + y_3 + y_4 \right]$$

$$\bar{z} = \frac{1}{4} \left[z_1 + z_2 + z_3 + z_4 \right]$$

Now the input points will be projected into the plane of the element along the normal vector. The resulting points are the corner points of the quadrilateral element. The input points are equidistant from the plane, and this distance is

$$d = \left| n_x(\bar{x} - x) + n_y(\bar{y} - y) + n_z(\bar{z} - z) \right|$$

The coordinates of the corner points in the reference coordinate system are given by

$$x'_k = x_k + (-1)^{k+1} n_x d$$

$$y'_k = y_k + (-1)^{k+1} n_y d \qquad k = 1, 2, 3, 4$$

$$z'_k = z_k + (-1)^{k+1} n_z d$$

The element coordinate system is now constructed. This requires the components of three mutually perpendicular unit vectors, one of which points along each of the coordinate axes of the system, and also the coordinates of the origin of the coordinate system. All these quantities must be given in terms of the reference coordinate system. The unit normal vector is taken as one of the unit vectors, so two perpendicular unit vectors in the plane of

the element are needed. Denote these unit vectors $\vec{t}_1$ and $\vec{t}_2$. The vector $\vec{t}_1$ is taken as $\vec{T}_1$ divided by its own length, T_1, i.e.,

$$t_{1x} = \frac{T_{1x}}{T_1}$$

$$t_{1y} = \frac{T_{1y}}{T_1}$$

$$t_{1z} = \frac{T_{1z}}{T_1}$$

where $\quad T_1 = \left[T_{1x}^2 + T_{1y}^2 + T_{1z}^2 \right]^{\frac{1}{2}}$

The vector $\vec{t}_1$ is defined by $\vec{t}_2 = n \times \vec{t}_1$, so that its components are

$$t_{2x} = n_y t_{1z} - n_z t_{1y}$$

$$t_{2y} = n_z t_{1x} - n_x t_{1z}$$

$$t_{2z} = n_x t_{1y} - n_y t_{1x}$$

The vector $\vec{t}_1$ is the unit vector parallel to the x or ξ axis of the element coordinate system, while $\vec{t}_2$ is parallel to the y or η axis, and $\vec{n}$ is parallel to the z or ζ axis of this coordinate system.

The corner points are now transformed into the element coordinate system based on the average point as origin. These points have coordinates x'_k, y'_k, z'_k in the reference coordinate system.

Their coordinates in the element coordinate system with this origin are denoted by ξ_k, η_k, 0. Becuase they lie in the plane of the element, they have a zero z or ζ coordinate in the element coordinate system. In the (ξ, η) coordinate system, the corner points of the element are:

$$\xi_k = t_{1x}(\bar{x} - x'_k) + t_{1y}(\bar{y} - y'_k) + t_{1z}(\bar{z} - z'_k)$$

$$\eta_k = t_{2x}(\bar{x} - x'_k) + t_{2y}(\bar{y} - y'_k) + t_{2z}(\bar{z} - z'_k)$$

These corner points are taken as the corners of a plane quadrilateral. The origin of the element coordinate system is now transferred to the centroid of the area of the quadrilateral. With the average point as origin, the coordinates of the centroid in the element system are:

$$\xi_0 = \frac{1}{3} \frac{1}{\eta_2 - \eta_4} \left[\xi_4 (\eta_1 - \eta_2) + \xi_2 (\eta_4 - \eta_1) \right]$$

$$\eta_0 = -\frac{1}{3} \eta_1$$

These are subtracted from the coordinates of the corner points in the element coordinate system based on the average point as origin to obtain the coordinates of the corner points in the element coordinate system based on the centroid as origin. Accordingly, these latter coordinates are

$$\xi_k = \xi_k - \xi_0$$

$$\eta_k = \eta_k - \eta_0$$

$$k = 1, 2, 3, 4$$

Since the centroid is to be used as the control point of the element, its coordinates in the reference coordinate system are requried. These coordinates are:

$$x_0 = \bar{x} + t_{1x}\xi_0 + t_{2x}\eta_0$$

$$y_0 = \bar{y} + t_{1y}\xi_0 + t_{2y}\eta_0$$

$$z_0 = \bar{z} + t_{1z}\xi_0 + t_{2z}\eta_0$$

Finally, the area of the quadrilateral is:

$$A = \frac{1}{2}(\xi_3 - \xi_1)(\eta_2 - \eta_4)$$

One additional rotation of the ξ, η axis is performed in order to ensure that the ξ, ζ phase is parallel to the reference x axis of the configuration.

The direction cosines of the axial vector, ℓ, and transverse vector, m, are given in terms of the normal vector, n, as follows:

$$\ell_x = \frac{n_z}{m_y} \qquad \ell_y = 0 \qquad \ell_z = \frac{-n_x}{m_y}$$

$$m_x = n_y\ell_z \qquad m_y = \sqrt{n_x^2 + n_z^2} \qquad m_z = -n_y\ell_x$$

APPENDIX II

INFLUENCE OF TIP AND TRAILING-EDGE VORTICES

The perturbation velocity components induced by the edge and trailing vortex systems associated with a vortex panel are derived in Reference 4. Formulas for constant and linearly varying vortices are listed below. The perturbation velocities are given at an arbitrary point, $P(x,y)$, and induced by a vortex which lies along the x axis between $x = 0$ and $x = \infty$.

Constant Line Vortex

$$u = 0$$

$$v = -\frac{z}{r^2}\left[1 + \frac{x}{d}\right]$$

$$w = \frac{y}{r^2}\left[1 + \frac{x}{d}\right]$$

where

$$r^2 = y^2 + z^2$$

and

$$d^2 = x^2 + r^2$$

Linearly Varying Line Vortex

$$u = 0$$

$$v = -\frac{z}{r^2} \left[x + d \right]$$

$$w = \frac{y}{r^2} \left[x + d \right]$$

For vortex panels having a constant distribution of vorticity, and non-parallel leading and trailing edges, a constant vortex sheet is generated and contained between the two trailing vortices in the wake. The perturbation velocities induced by this vortex sheet, which originates along the panel trailing edge and extends downstream to infinity are given below:

$$u = 0$$

$$v = -.5(B_{12} - B_{34})(F_3 + F_4)$$

$$w = .5(B_{12} - B_{34})(C_{43} \, G_{43} + H_{43})$$

where

$$H_{43} = \log \frac{x - \xi_4 + \sqrt{(x - \xi_4)^2 + r_4^2}}{x - \xi_3 + \sqrt{(x - \xi_3)^2 + r_3^2}} \cdot \frac{r_3}{r_4}$$

and B_{ij}, C_{ij}, F_i, G_{ij} are defined following equations (3) in the in the main text. The subscripts 3 and 4 refer to the outboard and inboard trailing edge corners of the vortex panel.

All of the above formulas are written assuming that the wake lies in the plane of the vortex panel, and that the edge and trailing vortices are parallel to the ξ axis of the panel. If the panel side edges or trailing vortices lie in the panel ξ,η plane, but are inclined at an angle, δ , with respect to the ξ axis, the following transformation applied:

$$u = u' \cos \delta - v' \sin \delta$$

$$v = v' \cos \delta + u' \sin \delta$$

$$w = w'$$

where u', v' and w' are the three components of velocity calculated in a primed coordinate system aligned with the vortex under consideration.